Tuning catalytic properties of bimetallic surfaces: Oxygen adsorption on pseudomorphic Pt/Ru overlayers

Markus Lischka and Axel Groß
Abteilung Theoretische Chemie, Universität Ulm, D-89069 Ulm, Germany
(Dated: October 4, 2005)

The adsorption of atomic and molecular oxygen on bimetallic Pt/Ru overlayer systems has been studied by periodic density functional theory calculations. A strong interaction between the Pt and the Ru layers is found resulting in a hcp stacking for the first Pt layer on Ru. The chemical properties of the Pt/Ru overlayers are beyond those of the single constituents Pt and Ru. Both the compression of the Pt overlayers as well as the strong direct interaction between Pt and Ru, which reaches up to the second Pt layer, reduce the atomic and molecular oxygen adsorption energies compared to pure Pt and Ru surfaces. Although the influence of the electrolyte and any external electric field are neglected, the results should still be relevant in the electrochemical context. The consequences of the theoretical findings for the oxygen reduction reaction in electrocatalysis are discussed.

Keywords: bimetallic surfaces, oxygen, platinum, ruthenium, density functional calculations, chemisorption

I. INTRODUCTION

Modifying the catalytic or electrocatalytic properties of a surface by systematically altering its electronic structure is an intriguing and fascinating idea. One way to achieve this goal is the application of external strain on the substrate [1–5]. Compressing or expanding any metal substrate changes the overlap of the atomic orbitals and thus consequently increases or decreases the width of the electronic bands. The effect of a lattice expansion on the *d*-band density of states of a transition metal such as ruthenium with a more than half-filled band is the following: Expanding the lattice to a larger lattice constant leads to less overlap and thus a narrowing of the *d*-band. This in turn causes an up-shift of the center of the *d* states in order to preserve the degree of *d*-band filling [2, 6]. The energetic position of the *d*-band center shifts closer to the Fermi level resulting in a larger reactivity according to the *d*-band model [7–9]. The reverse is true for compressed lattices: Compression causes a down-shift and thus a lower reactivity.

Experimentally, however, the application of external strain on a large scale is difficult. Metals easily form dislocations, and significant deformations are thus not possible. Nevertheless, it was shown experimentally [1, 10] that oxygen adsorption on Ru(0001) preferentially occurs on local areas with expanded lattices, whereas compressed lattice areas are depleted. In these experiments, the Ru surface layers were strained locally by argon implementation into subsurface cavities: At their rim, the lattice was compressed, whereas it was expanded at their top. Although these experiments proved the concept to be right, it does not allow for a quantitative assessment of the effect as the strain is only applied locally in a non-uniform way.

To achieve a macroscopic, uniformly strained surface, another approach has to be used: Growing a metal film pseudomorphically on top of a different metal substrate, it is possible to obtain overlayers compressed or expanded to the lattice constant of the underlying substrate. At some point, however, the strained layers will relax and continue to grow at their own lattice constant. Furthermore, the reactivity of the overlayers will not only be determined by the induced strain, but also by the electronic interaction of the overlayers with the underlying substrate. Of course, the thicker the overlayer is, the weaker will be the consequences of this interaction on the chemical properties of the overlayer system.

Pseudomorphic bimetallic overlayer systems have indeed recently attracted a lot of attention since they allow a systematic investigation of the relationship between the surface structure and composition and its chemical and catalytic properties [6, 11–23]. These studies have shown that the chemical and electrochemical properties of the bimetallic overlayer systems can significantly differ from those of the pure substrates.

In this paper, we examine the properties of the Pt/Ru(0001) overlayer system by performing periodic density functional theory (DFT) calculations. As shown experimentally , platinum overlayers deposited on a Ru(0001) grow pseudomorphically [12, 23–26], even up to a film thickness of 4 layers [12]. Compared to its own lattice constant, the platinum overlayers are compressed by 2.5% to adapt to the ruthenium lattice constant. This heteroepitaxial metal layer system thus allows for a discrimination between pure strain effects and effects due to a residual interaction with the underlying substrate. It has recently been shown that both the compression of the pseudomorphic Pt layers as well as the strong Pt-Ru interaction lead to reduced adsorption energies for CO [12, 27] and hydrogen [23].

In this study, we address the interaction of atomic and molecular oxygen with pseudomorphic Pt/Ru overlayers motivated by corresponding experiments [28]. This system is of particular interest since PtRu is regarded as a promising electrode material for the cathodic oxygen reduction reaction (ORR) [29]. In our calculations, the oxygen adsorption energies on Pt/Ru overlayers are de-

termined for the solid-vacuum interface so that the effects of the electrolyte and any external electric field are entirely neglected. However, the presence of an electrolyte such as water has only a weak influence on the binding energies in specific adsorption [30, 31]. Furthermore, theoretical predictions for the reactivity of bimetallic overlayers systems obtained at the solid-vacuum interface have recently been fully confirmed in an experimental electrochemical study [21]. Hence the results presented here will also be relevant for the electrochemical solid-liquid interface.

This paper is structured as follows. We will first discuss the pseudomorphic structure of the Pt/Ru overlayer system with up to five deposited layers of Pt, and then we will show how atomic and molecular oxygen adsorption is affected and modified by the film thickness. Finally we discuss the consequences of our findings for the oxygen reduction reaction on Pt/Ru overlayers.

II. COMPUTATIONAL DETAILS

All calculations reported in this article were performed using the Vienna *ab initio* simulation package (VASP) [32, 33] with the exchange-correlation effects treated within the so-called PW91 generalized gradient approximation (GGA) [34]. Where appropriate, the spin polarization has been included. The ionic cores are described by projector augmented wave (PAW) pseudopotentials [35, 36], with projections done in real space. The surface itself was modeled using supercells [37]. The Ru(0001) substrate was always represented by a four layer thick slab. On top of this substrate, one to five overlayers of laterally compressed Pt were considered (see Fig. 1). Denoting the number of grown Pt layers by n, we indicate the film thickness by nPt/Ru(0001) in our notation. For comparison, all adsorption calculations were also done on two four-layer slabs of platinum, one of which was unstrained with its computed nearest neighbor distance of bulk Pt, whereas the other was compressed horizontally to match the computed nearest neighbor distance of bulk Ru. The latter slab thus served as a model for an infinitely thick stack of laterally compressed Pt overlayers. Calculations using this compressed slab will be denoted as "Pt(111)@Ru". The separating vacuum region was chosen to be 12 Å and kept constant. The supercell size in the z direction perpendicular to the surface thus varied between 18.5 and 30.4 Å.

The Brillouin zone of the $p(1\times1)$ slab was sampled using a Γ-centered Monkhorst-Pack mesh of $12\times12\times1$ **k** points [38], together with a first-order Methfessel-Paxton smearing [39] of width $\sigma = 0.2$ eV. Reported total energies are extrapolated to $\sigma \to 0$ eV. The valence states were expanded in a basis of plane waves with kinetic energies below 290 eV. For adsorption calculations using a $p(2\times2)$ surface unit cell, a Monkhorst-Pack mesh of $4\times4\times1$ **k** points and, due to the harder oxygen core, a higher energy cut-off of 400 eV were necessary to obtain converged total energies. Geometrical relaxations were carried out using the Hellman-Feynman forces and a conjugate-gradient minimization scheme. In all calculations, the two bottom Ru or Pt layers were kept fixed at their truncated bulk positions whereas all other layers were relaxed such that the forces on each atom were below 0.02 eV/Å.

Lattice constants for both bulk platinum and ruthenium were obtained by fitting the Murnaghan equation of state [41, 42] to the computed total energies at several different lattice parameters. For the hexagonal lattice of ruthenium, both lattice parameters a and c would need to be optimized. However, as a previous VASP study [43] showed that the c/a ratio obtained by a full optimization using the GGA functional is $c/a = 1.58$, we kept the c/a ratio fixed to the experimental value of $c/a = 1.582$. The theoretical Ru nearest neighbor distance was then determined to be 2.73 Å, a bit larger (1.1%) than the experimental value (see Table I). For Pt, a lattice constant of 3.99 Å was calculated in comparison to a slightly smaller (1.8%) experimental value of 3.92 Å. The in-plane Pt-Pt nearest neighbor distance of an unstrained Pt(111) slab is thus 2.82 Å. Both determined lattice constants are within the expected accuracy of the GGA exchange-correlation functional. Due to the different absolute deviations, the lattice mismatch of the theoretically computed lattice constants amounts to 3.2%, whereas the experimental lattice mismatch is only 2.6%. The effect of compressing the platinum layer to match the ruthenium lattice might thus be slightly overestimated within the GGA approximation.

III. RESULTS AND DISCUSSION

A. PtRu stacking

When pseudomorphically growing a platinum overlayer on Ru(0001), the platinum atoms of the first overlayer can be either adsorbed in fcc hollow or hcp hollow positions. To determine the correct layer stacking with the lowest energy, all possible permutations for adsorption of each additional platinum overlayer were computed. Referring to the top two Ru layers as AB as denoted in

TABLE I: Bulk properties of Pt and Ru as determined self-consistently by GGA-PAW calculations. Experimental data is taken from [40]. The c/a ratio of ruthenium was fixed to the experimental value.

	Ru		Pt	
	a [Å]	c/a	a [Å]	B_0 [GPa]
GGA-PAW	2.73	1.582	3.99	231
Exp.	2.70		3.92	230

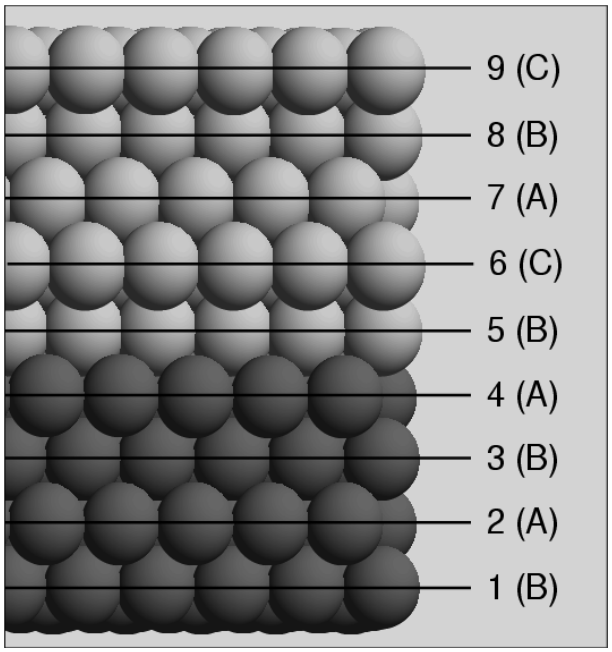

FIG. 1: Stacking sequence of pseudomorphic platinum overlayers on Ru(0001). The first platinum layer (layer no. 5) continues the hexagonally close-packed structure of ruthenium (sequence AB). Beginning with the sixth layer, platinum starts to grow in its face-centered cubic structure (ABC sequence). Reported layer spacings refer to the layer numbers shown in the illustration.

Fig. 1, with the top layer being A, epitaxial growth of Pt can continue the stacking as either BAB (hcp hollow adsorption) or BAC (fcc hollow position). For the first overlayer, continuation of the hexagonally closed packed structure of Ru, sequence BAB, is favorable by 18 meV per $p(1 \times 1)$ surface unit cell compared to the sequence BAC. Starting with the second layer of platinum, however, growth switches to the face-centered cubic structure of bulk Pt. Adsorption of the second overlayer resulting in a stacking of BABC is energetically favored by 31 meV in comparison to the next best structure of BABA. Starting with the third overlayer, the platinum layers, although compressed by 3.2%, grow according to the fcc stacking found for bulk Pt. The lowest energy structure found for 5Pt/Ru(0001) is illustrated in Fig. 1. All further adsorption calculations will be performed using the discussed Pt film structure.

At all film thicknesses, a full relaxation of the Pt overlayers and the two top-most Ru layers was allowed. The computed interlayer distances are summarized in Table II. The topmost Ru-Ru interlayer spacing, d_{3-4}, is found to be contracted by 3.7% to 2.08 Å, which is somewhat larger than the LEED-determined value of 2.3% [44]. Upon adsorption of Pt overlayers, this contraction is slightly reduced to 2.11 Å. The interlayer distance of the first Pt overlayer to the Ru substrate is initially found to be 2.31 Å and is further reduced to 2.28 Å as more Pt layers are grown on top. This Pt-Ru interlayer distance is almost identical to the interlayer distance of bulk Pt(111), $d_{\mathrm{Pt(111)}} = 2.30$ Å, although the layer is compressed significantly in-plane. Starting with the second Pt layer, the Pt-Pt interlayer distance is found to be approximately 2.41 Å, almost identical up to a film thickness of 5 layers within the accuracy of our numerical calculations. The lateral compression is thus compensated for by an increase of the layer distance from 2.30 Å to 2.41 Å.

Also given in Table II is the separation energy of each Pt overlayer. The separation energy is defined as the energy needed to completely separate the top-most layer from its remaining substrate while keeping the in-plane nearest-neighbor distances fixed. It is thus an indication of the strength of the chemical interaction between the surface layer and the substrate. For the first Pt overlayer, a rather large separation energy of 1.57 eV/atom is found, whereas adsorption of additional overlayers yields an almost constant energy gain of roughly 0.93 eV/atom. This shows that there is a strong attractive interaction between the Pt and the Ru atoms. It has to be noted that the separation energy does not take into account any energy released due to the "assembly" of the free Pt monolayer: Compared to bulk Pt(111), a free monolayer of Pt actually tries to contract itself to compensate for the lack of bonding partners above and below. Compressing a free Pt(111) monolayer from its bulk lattice constant to the Ru lattice constant of 2.73 Å gives an energetical gain of $\Delta E = 0.24$ eV, with the energetic minimum being located at an even smaller Pt-Pt distance of approximately 2.62 Å [45]. In this sense, the surface termination of 1Pt/Ru(0001) is much more "ideal" for the top Pt layer than in uncompressed Pt(111). This is also true for the other nPt/Ru(0001) systems and for

TABLE II: Layer relaxations of the system nPt/Ru(0001). Reported layer distances d_{n-m} refer to the layer numbers given in Fig. 1. Printed in italics is the layer distance between the Ru substrate and the first Pt overlayer, d_{4-5}. For comparison, the interlayer distance of Ru(0001) at its bulk-truncated positions is $d_{\mathrm{Ru(0001)}} = 2.16$ Å (Exp. 2.14 Å [44]), that of Pt(111) $d_{\mathrm{Pt(111)}} = 2.30$ Å (Exp. 2.26 Å [40]). Also given is the energy to completely separate the top-most overlayer from the rest of the slab, ΔE_{sep}.

nPt/Ru(0001)	0	1	2	3	4	5
d_{8-9} (Å)						2.41
d_{7-8} (Å)					2.41	2.40
d_{6-7} (Å)				2.42	2.41	2.41
d_{5-6} (Å)			2.41	2.40	2.40	2.41
d_{4-5} (Å)		*2.31*	*2.25*	*2.28*	*2.27*	*2.28*
d_{3-4} (Å)	2.08	2.08	2.11	2.11	2.10	2.11
d_{2-3} (Å)	2.14	2.14	2.13	2.13	2.13	2.13
ΔE_{sep} (eV/atom)		1.57	0.92	0.92	0.93	0.94

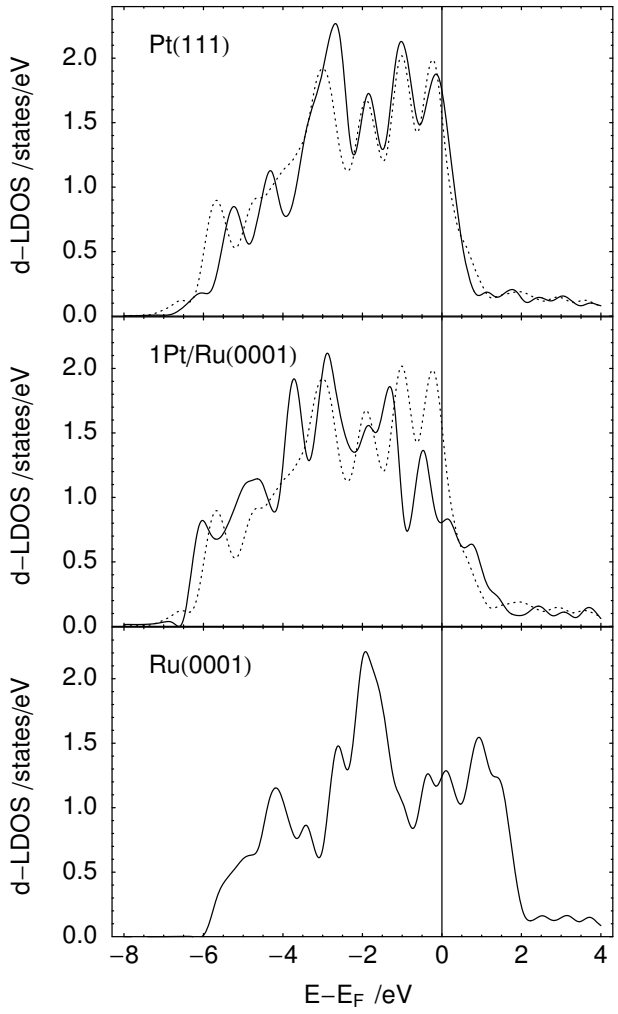

FIG. 2: Local d-band density of states of nPt/Ru(0001). From top to bottom, the d-band LDOS of the surface layer of Pt(111), 1Pt/Ru(0001), and Ru(0001) are shown. For comparison, the LDOS of the compressed surface layer of the Pt(111)@Ru slab is also plotted as a dashed line.

Pt(111)@Ru.

From the given structural data, it can thus be inferred that, starting with the third layer, growth of additional platinum overlayers is not influenced by electronic interactions with the Ru substrate any more. Growth is then only affected by the strain due to the pseudomorphic growth.

As discussed in the introduction, the reactivity of a system, especially under strain, is mostly influenced by the d-band valence states, the key parameter being their energetic center, ε_d. The local d-band densities of states of the surface layers of Pt(111), Pt(111)@Ru, 1Pt/Ru(0001), and Ru(0001) are displayed in Fig. 2. The top panel shows both the d-LDOS of unstrained (solid line) and compressed (dashed line) Pt(111). Due to the compression and increased overlap, the d-band gets significantly broadened. Adsorption of a monolayer of Pt on Ru(0001) even further modifies the d-band distribution (middle panel of Fig. 2): Interaction with the Ru substrate reduces the density of states at the Fermi level and causes a further overall down-shift of the valence states, again indicating the strong interaction between Pt and Ru.

This downshift can be quantified by determining the energetic position of the d-band center. For an accurate determination of the d-band center, a larger $\mathbf{k}$ point mesh of $16 \times 16 \times 1$ was used and the number of bands was increased to make sure that all relevant states above the Fermi level are included. To avoid picking up any irrelevant noise above the actual d band due to the projection scheme, the integrals necessary to determine the d-band centers were truncated at the upper edge of the d-band. The d-band centers computed are summarized in Table III. As expected from Fig. 2, the compression of Pt(111) to the Ru nearest neighbor distance causes a noticeable downshift of the d-band center from -2.23 eV to -2.37 eV. However, the influence of the Ru substrate on the first Pt overlayer is even stronger: Hybridization with the Ru orbitals lowers the d-band center to -2.61 eV. Within the numerical accuracy, the d-band centers of the top layer of the systems Pt(111)@Ru and nPt/Ru(0001) with $n = 2 \ldots 5$ do not exhibit significant differences. Considering thus only the top layer, the chemical reactivity of these systems should roughly be the same.

Finally, this trend is also confirmed by looking at the work function change with growing film thickness. The work function is computed by introducing a dipole layer in the vacuum region. As given in Table III, the work function continually increases going from pure Ru(0001) over 1Pt/Ru(0001) and 2Pt/Ru(0001) to 3Pt/Ru(0001). From then on, the work function remains roughly constant with a value slightly larger than the one of unstrained Pt(111).

Based on the properties of the clean nPt/Ru(0001), we can thus conclude that the influence of the Ru substrate should be negligible starting with the third Pt layer. For

TABLE III: of nPt/Ru(0001). Experimental data is taken from [46] and represents orientation-specific measurements. For Pt(111), two different experimental values are quoted.

		Φ /eV	
	ε_d /eV	Theory	Exp.
Ru(0001)	-1.54	5.12	5.37
1Pt/Ru(0001)	-2.61	5.46	
2Pt/Ru(0001)	-2.38	5.71	
3Pt/Ru(0001)	-2.32	5.88	
4Pt/Ru(0001)	-2.35	5.82	
5Pt/Ru(0001)	-2.36	5.85	
Pt(111)@Ru	-2.37	5.84	
Pt(111)	-2.23	5.80	5.93 / 5.82

$n = 1$, we expect a large modification of adsorption properties due to the observed strong interaction of the Pt monolayer with the Ru substrate. Starting with $n = 3$, however, residual interactions should have vanished and the remaining modifications should solely be due to the strain on the Pt layers.

B. Atomic adsorption of oxygen

Oxygen adsorption on Pt(111) is a well-studied system, both experimentally [47–54] and theoretically [55–62]. It is well established that, at a coverage of $\theta = 0.25$, oxygen forms a $p(2 \times 2)$ superstructure with the oxygen atoms being adsorbed in fcc hollow positions (no atom in the layer beneath the site). On the other hand, on Ru(0001), again a $p(2\times2)$ superstructure is found, but with the oxygen atoms occupying hcp hollow positions [63–65]. In the following, we will thus check how the application of strain and the residual interaction of the ruthenium substrate influences the adsorption of a $p(2 \times 2)$ layer of atomic oxygen.

Adsorption energies of oxygen will be reported with respect to the free O_2 molecule in the gas phase. Oxygen is known to be problematic within the DFT pseudopotential approach due to its hard core. It is the main reason for the relatively large energy cut-off of 400 eV in our calculations. The O_2 ground state properties were obtained from a Morse potential fit and are compared to the experimental data in Table IV. Although the binding energy obtained using ultrasoft pseudopotentials is significantly closer to the experimental value, the PAW result is indeed very close to all-electron calculations for O_2 [67]. It is thus only by chance that the induced error due to a softer, inaccurate core region counterbalances the DFT error due to the exchange-correlation functional. We have used PAW potentials throughout this work and refer adsorption energies to the PAW binding energy of $E_b = 6.27$ eV.

Final adsorption energies for oxygen in the fcc hollow, hcp hollow, and bridge sites are displayed in Fig. 3. All atoms except the two bottom slab layers were allowed to relax completely. In the case of bridge adsorption, the oxygen atom was fixed laterally, though. Adsorption energies for the fcc hollow position are also listed in Table V together with the computed oxygen-metal distances. All

TABLE IV: Binding energy, bond length, and stretching frequency for the O_2 molecule. Experimental data is taken from Ref. [66].

O_2	E_b /eV	d /Å	ω /cm^{-1}
GGA-USPP	5.86	1.24	1572
GGA-PAW	6.27	1.24	1567
Exp.	5.21	1.21	1580

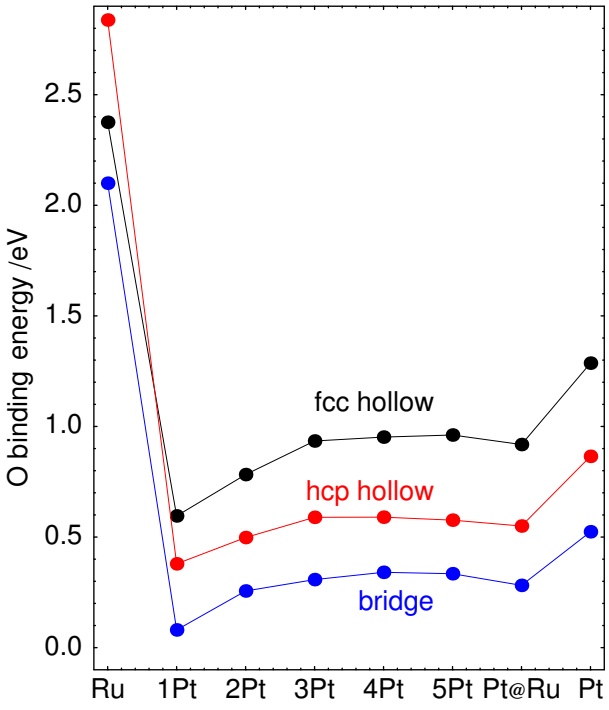

FIG. 3: Adsorption energies of $p(2 \times 2)$-O/nPt/Ru(0001). The energies per atom for adsorption in the fcc hollow, hcp hollow and bridge sites are shown with respect to free O_2 molecule. Energies on the strained Pt slab are denoted as "Pt@Ru", on the uncompressed Pt slab as "Pt". Except for Ru(0001), adsorption in the fcc hollow site is energetically favorable. Binding energies with respect to free atomic O may be obtained by adding half the binding energy of O_2, 3.13 eV, to the given binding energy.

relaxations yielded a small buckling of the surface layers on the order of 0.1 Å, in good agreement with the observed small buckling on both the Ru(0001) [63] and Pt(111) [50, 51] surfaces. The height of the oxygen atom, $\Delta z_{\mathrm{O-Me}}$, given in Table V, is calculated using the relaxed nearest neighbor distances, i.e., the height of the oxygen atom with respect to the clean surface is slightly larger due to the outward relaxation of the nearest neighbors.

Ignoring the binding energies on clean Ru(0001), all three energy curves in Fig. 3 show the same trend: Compressing the platinum slab to the Ru lattice constant, decreases the adsorption energy by roughly 0.3 eV. A monolayer of Pt on top of Ru(0001) exhibits another drastic reduction in binding energy by 0.3 eV compared to the compressed Pt(111) slab. The systems with 3 to 5 layers of platinum yield roughly the same adsorption energy as the strained Pt slab, whereas adsorption energies on the 2Pt/Ru(0001) system are still significantly reduced. This clearly shows that the electronic properties of the second layer atoms are still modified by the presence of

the substrate as also found for other systems [13, 14, 68].

The compression of the Pt(111) surface also alters the vibrational properties of the adsorbed oxygen atom. On the unstrained Pt(111), by using a cubic fit to the total energies at elongated positions of $\Delta z = 0.00, \pm 0.05$, and ± 0.10 Å, we obtain a vibrational frequency for the symmetric mode perpendicular to the surface of 448 cm^{-1}. This is somewhat lower than the value of 475 cm^{-1} obtained using the LDA approximation [57] or the value of 477 cm^{-1} found experimentally [47, 53]. Nevertheless, all theoretically reported frequencies do not take into account the finite mass of the substrate atoms. By using a simple spring model for the threefold hollow adsorption scenario, the first-order correction due to the finite mass of the substrate atoms can be found to be [69]

$$\omega = \omega(M_s \to \infty)\sqrt{1 + \frac{M_a}{3M_s \cos^2 \alpha}}, \qquad (1)$$

where $\omega(M_s \to \infty)$ is the frequency obtained in the limit of infinite substrate mass, M_a and M_s are the mass of the adsorbate and substrate atoms, respectively, and $\cos\alpha = \frac{\Delta z_{\mathrm{O-Me}}}{d_{\mathrm{O-Me}}}$. Applying this correction formula to our computed frequency gives $\omega = 467$ cm^{-1}, in much better agreement with the experimentally observed frequency. On the compressed Pt(111) surface, the frequency is increased to 485 cm^{-1} (503 cm^{-1} after finite mass correction). Experimentally, a similar trend towards a higher frequency is observed, but only with a very small shift to $\omega = 483.7$ cm^{-1} [24].

So far, we did not discuss oxygen adsorption on Ru(0001): As can be seen in Fig. 3, adsorption of oxygen in the hcp hollow positions is favored by 0.46 eV ($E_b = 2.84$ eV) in contrast to the opposite ordering on Pt(111) where the fcc hollow position is preferred by 0.42 eV. For 1Pt/Ru(0001) and 2Pt/Ru(0001) the preferential occupation of the fcc hollow site is already weakened by the influence of the underlying Ru substrate as can be inferred from the decreasing energy difference between fcc hollow and hcp hollow adsorption energies.

TABLE V: Adsorption energies and geometries for $p(2\times2)$-O/nPt/Ru(0001) for adsorption in the fcc hollow position. Listed are the binding energy per oxygen atom with respect to the free O_2 molecule, E_b, the oxygen-metal distance, $d_{\mathrm{O-Me}}$, the height of the oxygen atom above the top-most metal atom, $\Delta z_{\mathrm{O-Me}}$, and the characteristic frequency for vibrations along the surface normal, ω. Frequencies in parentheses are corrected for the finite mass of the substrate atoms.

	E_b [eV]	$d_{\mathrm{O-Me}}$ [Å]	$\Delta z_{\mathrm{O-Me}}$ [Å]	ω [cm^{-1}]
Ru(0001)	2.38	2.03	1.14	
1Pt/Ru(0001)	0.60	2.10	1.36	
2Pt/Ru(0001)	0.78	2.05	1.26	
3Pt/Ru(0001)	0.93	2.05	1.25	487 (504)
4Pt/Ru(0001)	0.95	2.05	1.25	
5Pt/Ru(0001)	0.96	2.05	1.25	
Pt(111)@Ru	0.92	2.04	1.25	485 (503)
Pt(111)	1.29	2.04	1.14	448 (467)

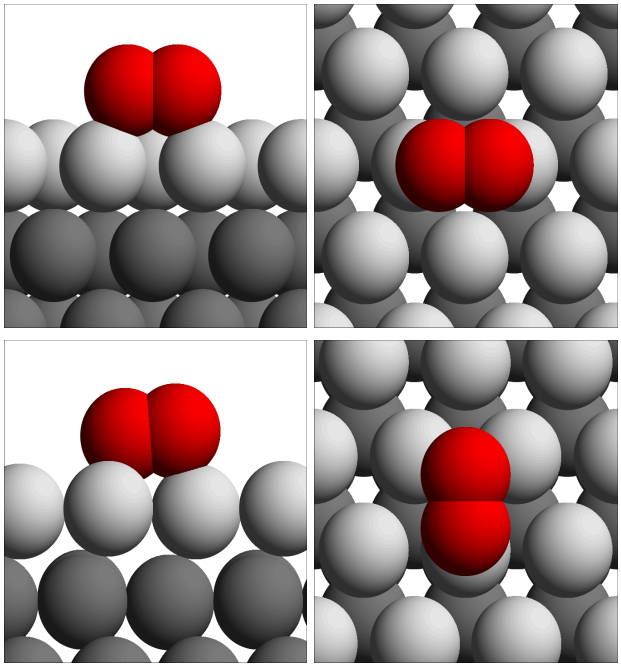

FIG. 4: Structure of the oxygen molecular adsorption states. Top panels: Side and top view of the O_2^- molecular precursor state (superoxo state) on the 1Pt/Ru(0001) surface. The orientation of the O_2 molecule is t-b-t. Bottom panels: Side and top view of the O_2^{2-} molecular precursor state (peroxo state). The orientation is b-fcc-t, and the molecule on a fully relaxed surface is tilted by 7° off the (111) plane.

C. Molecular adsorption of O_2

Atomic oxygen adsorption on Pt(111) is known to be mediated by molecular precursors [47, 49, 62, 70–72]. In experiments, two distinct molecular precursors were identified [47, 49, 70]: A superoxo-like (O_2^-) species formed at bridge sites with an intramolecular bond order of 1.5 and a vibrational frequency of 870 cm^{-1}, and a peroxo-like (O_2^{2-}), slightly stronger bound species adsorbed at threefold hollow sites exhibiting an intramolecular bond order of 1 and a vibrational frequency of 690 cm^{-1}.

Theoretical GGA-DFT studies corroborated this hypothesis [58, 61]: The superoxo precursor state was found to be adsorbed in a top-bridge-top (t-b-t) orientation on the Pt(111) surface which means that the center of mass of the O_2 molecule is located above the bridge site with the two O atoms oriented towards the adjacent top sites (see Fig. 4). In this configuration, the chemisorbed O_2 molecule has a remaining magnetic moment of $m_{O_2} = 0.4\mu_B$. The peroxo molecular precur-

sor, on the other hand, is identified as being adsorbed non-magnetically in a top-fcc hollow-bridge (t-fcc-b) orientation. The peroxo species is slightly tilted off the (111) plane. The PW91-GGA calculations [58] yielded adsorption energies of $E_b = 0.72$ eV and $E_b = 0.68$ eV for the superoxo and peroxo species, respectively. Experimentally, the adsorption energies were estimated to be approximately 0.5 eV [47], and it has to be noted that the uncertainty due to the approximative exchange-correlation functional is rather large for systems involving oxygen. This can already be seen from the substantial error in the binding energy of O_2 (see Table IV), and resulting binding energies computed with different exchange-correlation functionals vary widely. Computations using the RPBE functional, e.g., yield much lower binding energies of $E_b \approx 0.1$ eV only [73, 74].

The molecular adsorption calculations were done in a $p(2 \times 2)$ geometry. This effectively doubles the oxygen coverage per cell in comparison to the previous section, but interaction of neighboring O_2 molecules are still considered to be small. In contrast to the original study of O_2 on Pt(111) by [58], we do not use a $\sqrt{3} \times 2$ unit cell. Using this rectangular cell does not represent the C_{3v} symmetry of the hexagonal Ru lattice accurately. With no adsorbate present, the **k** point mesh is symmetrized accordingly. But as soon as an oxygen molecule is present, the C_{3v} symmetry is broken and **k** vectors along the two surface unit cell vectors are no longer equivalent. For larger slabs of nPt/Ru(0001) with $n > 2$, this turned out to be a significant disadvantage as rather large numerical drifts in the computed Hellman-Feynman forces rendered relaxations for such slabs useless. In a $p(2 \times 2)$ geometry, both unit cell directions and thus **k** points along them are related by the intrinsic symmetry of the slab. Therefore, any symmetry violations of the computed forces are avoided.

On the unstrained Pt(111) slab, the binding energies of O_2 are determined to be almost degenerate, i.e., $E_b = 0.80$ eV and $E_b = 0.78$ eV for the O_2^{2-} peroxo and the O_2^- superoxo precursor, respectively. The energetical ordering of the two molecular precursor states is thus reverted in comparison to the original $\sqrt{3} \times 2$ results cited above [58]. Due to the different geometry, this might be simply attributed to O-O repulsion effects, as the O-O distance of neighboring peroxo precursors is changed from roughly 3.5 Å in a $\sqrt{3} \times 2$ unit cell to 4.5 Å in a $p(2 \times 2)$ unit cell.

All results for nPt/Ru(0001) are summarized in Fig. 5 and Table VI. The expected trend of decreasing reactivity and lower binding energies going from Pt(111) over compressed Pt(111) to 1Pt/Ru(0001) is again observed. For all nPt/Ru(0001) surfaces, the superoxo precursor is slightly stronger bound than the peroxo precursor contrary to unstrained Pt(111). For the t-b-t orientation of the superoxo precursor, compressing the lattice constant seems to be more favorable as it allows the molecule to adsorb with a slightly smaller O-O bond length.

For the O_2^- superoxo precursor, we have also determined magnetic moments and vibrational frequencies. The magnetic moments given are total magnetic moments of the whole slab, with most of the polarized charge located at the oxygen atoms. The spin polarization of the adsorbed O_2 molecule is clearly correlated with its binding energy: The weaker the binding to the metal substrate, the more of the gas phase polarization of $\mu = 2\mu_B$ is preserved. Vibrational frequencies were obtained using a cubic fit to the total energies at elongated positions $\Delta d_{O-O} = 0.0, \pm 0.05, \pm 0.10$ Å and reveal a similar correlation to the binding energy: With increasing spin compensation of the O_2 molecule, i.e., with increasing occupation of the π^* antibonding O_2 orbitals, the O-O bond gets weakened and the vibrational frequency gets more and more reduced from the gas phase value of $\omega = 1567$ cm^{-1}.

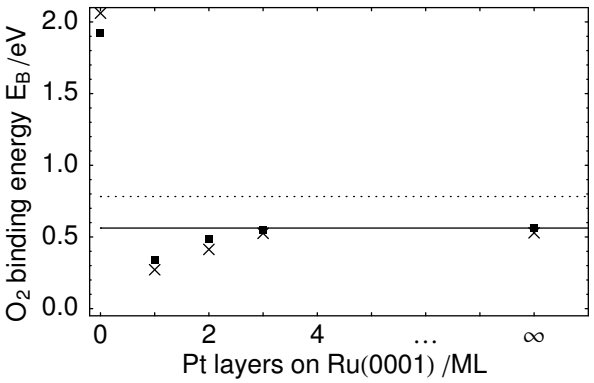

FIG. 5: O_2 molecular adsorption energies on nPt/Ru(0001) using a $p(2 \times 2)$ surface unit cell. Both adsorption energies of the O_2^- superoxo precursor (solid box) and the O_2^{2-} peroxo precursor (×) are shown. The solid line marks the final adsorption energy of O_2^- for compressed Pt(111). The adsorption energy of the O_2^- superoxo precursor on unstrained Pt(111) is indicated by the dashed line.

TABLE VI: Adsorption energies and geometries for molecular oxygen adsorption on nPt/Ru(0001). Binding energies and bond lengths for both the O_2^{2-} peroxo and the O_2^- superoxo precursor are given. For the spin-polarized O_2^- state, total magnetic moments and stretching frequencies are also reported.

	O_2^{2-}		O_2^-			
	E_b/eV	d_{O-O}/Å	E_b/eV	d_{O-O}/Å	μ/μ_B	ω/cm^{-1}
Ru(0001)	2.06	1.48	1.92	1.42	0.00	749
1Pt/Ru(0001)	0.27	1.38	0.34	1.34	0.82	1007
2Pt/Ru(0001)	0.41	1.38	0.48	1.34	0.75	961
3Pt/Ru(0001)	0.53	1.39	0.55	1.36	0.70	913
Pt(111)@Ru	0.53	1.38	0.56	1.35	0.79	940
Pt(111)	0.80	1.40	0.78	1.36	0.61	908

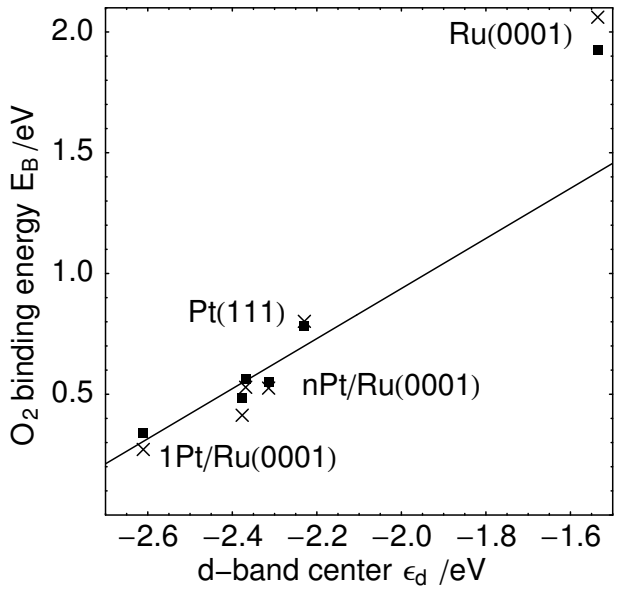

FIG. 6: Molecular O_2 adsorption energy versus d-band center (with respect to the Fermi energy) of the surface Pt atom for a $p(2 \times 2)$ ordered overlayer. Both adsorption energies of the O_2^- superoxo precursor (solid box) and the O_2^{2-} peroxo precursor ($\times$) are shown. The solid line represents the best least-squares linear fit to the O_2^- energies [excluding the one on Ru(0001)].

Similar to the results of atomic oxygen adsorption, both effects of compressing the Pt(111) surface by 3.2% and interactions with the Ru substrate are clearly separable. In both cases, the compression by 3.2% and the influence of the Ru(0001) on the first Pt monolayer yields roughly the same change in adsorption energies. As shown in Sec. III A, both the compression of Pt(111) monolayers and the strong inter-layer bonding between the two metals drastically modifies the distribution of the d-band valence states as shown in Fig. 2. According to the Hammer-Nørskov model [7–9], the O_2 adsorption energy should be directly proportional to the center of the locally projected d-band of the surface atom. In Fig. 6, the d-band center of the top-layer atom, ε_d, is plotted against the computed binding energies for the O_2^{2-} peroxo and the O_2^- superoxo precursors (see also Table III and VI). Also drawn is the best least-squares linear fit to the O_2^- binding energies on all systems with a Pt top-layer atom. The binding energy of O_2^- on Ru(0001) is somewhat offset from this trend, as might be expected from the Hammer-Nørskov d-band model [7–9] since the coupling matrix elements between O and Ru on the one hand and O and Pt on the other hand are different so that the simple linear relationship between d-band center and binding energy is not valid if oxygen adsorption on Ru and on Pt is compared. Nevertheless, the correct trend for the adsorption of O_2 on the different nPt/Ru(0001) systems is clearly reproduced.

Experimental adsorption energies for O_2 on nPt/Ru(0001) are not available. Initial sticking coefficients were, however, determined recently [28]. The experiments yield that the O_2 sticking coefficient rises with the number n of the Pt overlayers. This is in qualitative agreement with the results of our calculations since usually the molecular sticking probability rises with increasing binding energies of the impinging molecules [75].

Applying the same trend to the case of CO, the decrease in the adsorption energy on the PtRu overlayers would reduce the CO coverage and thus also reduce the blocking effect of CO in electrocatalysis and fuel cells leading to CO poisoning. As far as the oxygen reduction reaction in electrocatalysis is concerned, the exact microscopic mechanism is still controversely discussed [29, 76, 77]. The reaction should involve the breaking of the O-O bond and the formation of an O-H bond. Like in any catalytic reaction, the reactands have to interact strongly enough with the catalyst surface so that the barriers for bond breaking and making are reduced, but the reaction products should be bound weakly enough so that they can be efficiently released from the surface. Hence any catalytic process relies on a delicate balance requiring an intermediate interaction strength.

In a recent electrocatalytic study, a platinum monolayer supported on Ru(0001) showed a very low activity for the oxygen reduction, much lower than pure Pt(111) or a monolayer of Pt supported on Pd(111) [29]. On the other hand, the production of H_2O_2 was found to be larger on Pt/Ru(0001) than on other platinum monolayers. The small adsorption energies for atomic and molecular oxygen found in this study indicate that there is only a weak interaction between oxygen and one monolayer of Pt on Ru(0001). Obviously, this interaction is too weak in order to efficiently induce the O-O breaking thus making 1Pt/Ru(0001) an unsuitable catalyst for the oxygen reduction reaction. This weak interaction is also reflected in the adsorption experiments [28]. It would certainly be interesting to experimentally check the catalytic activity of the nPt/Ru(0001) overlayer systems for the oxygen reduction reaction as a function of the number of Pt overlayers since the reactivity of these overlayer systems increases with the number of Pt layers.

IV. CONCLUSIONS

We have addressed the adsorption of atomic and molecular oxygen on pseudomorphic Pt layers deposited on Ru(0001) for up to five Pt layers by performing density functional theory calculations. Both the compression of the pseudomorphic Pt layers by 3.2 % as well as the strong interaction between Pt and Ru lead to reduced oxygen adsorption energies on the PtRu overlayers. The direct interaction between the Pt overlayers and the Ru substrate is significant for up to the second Pt layer. It is important to note that the properties of the PtRu

overlayer systems are not intermediate between those of the two constituents. They rather bind adsorbates less strongly than the two elementary metals.

These weaker binding energies would be beneficial as far as the CO poisoning of catalysts is concerned because it would reduce the equilbrium CO coverage and thus its blocking effect. In the case of the oxygen reduction reaction, the interaction of one monolayer of Pt on Ru(0001) with oxygen is too weak to induce the O-O bond breaking of molecular oxygen. Still the PtRu overlayer system might be suitable as a catalyst for the oxygen reduction reaction for a larger number of Pt overlayers since its interaction strength increases with the number of Pt overlayers.

Acknowledgements

We thank Andreas Schlapka and Peter Jakob for useful discussions and for sharing their results with respect to the O_2 adsorption on the PtRu overlayers with us prior to publication.

[1] M. Gsell, P. Jakob, and D. Menzel, Science **280** (1998) 717.
[2] M. Mavrikakis, B. Hammer, and J. K. Nørskov, Phys. Rev. Lett. **81** (1998) 2819.
[3] J. Wintterlin, T. Zambelli, J. Trost, J. Greeley, and M. Mavrikakis, Angew. Chem. Int. Ed. **42** (2003) 2850.
[4] S. Sakong and A. Groß, Surf. Sci. **525** (2003) 107.
[5] S. Sakong and A. Groß, J. Catal. **231** (2005) 420.
[6] A. Ruban, B. Hammer, P. Stoltze, H. L. Skriver, and J. K. Nørskov, J. Mol. Catal. A **115** (1997) 421.
[7] B. Hammer and J. K. Nørskov, Surf. Sci. **343** (1995) 211.
[8] B. Hammer, Y. Morikawa, and J. K. Nørskov, Phys. Rev. Lett. **76** (1996) 2141.
[9] B. Hammer, O. H. Nielsen, and J. K. Nørskov, Catal. Lett. **46** (1997) 31.
[10] P. Jakob, M. Gsell, and D. Menzel, J. Chem. Phys. **114** (2001) 10075.
[11] A. Groß, Top. Catal., in press.
[12] A. Schlapka, M. Lischka, A. Groß, U. Käsberger, and P. Jakob, Phys. Rev. Lett. **91** (2003) 016101.
[13] A. Roudgar and A. Groß, Phys. Rev. B **67** (2003) 033409.
[14] A. Roudgar and A. Groß, J. Electroanal. Chem. **548** (2003) 121.
[15] A. Roudgar and A. Groß, Surf. Sci. **559** (2004) L180.
[16] T. E. Shubina and M. T. M. Koper, Electrochim. Acta **47** (2002) 3621.
[17] M. T. M. Koper, Surf. Sci. **548** (2004) 1.
[18] J. R. Kitchin, J. K. Norskøv, M. A. Barteau, and J. G. Chen, Phys. Rev. Lett. **93** (2004) 156801.
[19] M. Baldauf and D. M. Kolb, J. Phys. Chem. **100** (1996) 11375.
[20] L. A. Kibler, M. Kleinert, V. Lazarescu, and D. M. Kolb, Surf. Sci. **498** (2002) 175.
[21] L. A. Kibler, A. M. El-Aziz, R. Hoyer, and D. M. Kolb, Angew. Chemie, Int. Ed. **44** (2005) 2080.
[22] F. Maroun, F. Ozanam, O. M. Magnussen, and R. J. Behm, Science **293** (2002) 1811.
[23] H. Hoster, B. Richter, and R. J. Behm, J. Phys. Chem. B **108** (2004) 14780.
[24] A. Schlapka, U. Käsberger, D. Menzel, and P. Jakob, Surf. Sci. **502** (2002) 129.
[25] U. Käsberger and P. Jakob, Surf. Sci. **540** (2003) 76.
[26] T. Lei, M. S. Zei, and G. Ertl, Surf. Sci. **581** (2005) 142.
[27] F. Buatier de Mongeot, M. Scherer, B. Gleich, E. Kopatzki, and R. J. Behm, Surf. Sci. **411** (1998) 249.
[28] A. Schlapka, *Adsorption von CO und O_2 auf Pt/Ru(001) Bimetalloberflächen*, PhD thesis, Technische Universität München, 2002.
[29] J. L. Zhang, M. B. Vukmirovic, Y. Xu, M. Mavrikakis, and R. R. Adzic, Angew. Chem. Int. Ed. **44** (2005) 2132.
[30] A. Roudgar and A. Groß, Chem. Phys. Lett. **409** (2005) 157.
[31] A. Roudgar and A. Groß, Surf. Sci., in press.
[32] G. Kresse and J. Furthmüller, Phys. Rev. B **54** (1996) 11169.
[33] G. Kresse and J. Furthmüller, Comput. Mater. Sci. **6** (1996) 15.
[34] J. P. Perdew, J. A. Chevary, S. H. Vosko, K. A. Jackson, M. R. Pederson, D. J. Singh, and C. Fiolhais, Phys. Rev. B **46** (1992) 6671.
[35] P. E. Blöchl, Phys. Rev. B **50** (1994) 17953.
[36] G. Kresse and D. Joubert, Phys. Rev. B **59** (1999) 1758.
[37] A. Groß, Surf. Sci. **500** (2002) 347.
[38] H. J. Monkhorst and J. D. Pack, Phys. Rev. B **13** (1976) 5188.
[39] M. Methfessel and A. T. Paxton, Phys. Rev. B **40** (1989) 3616.
[40] C. Kittel, *Introduction to Solid State Physics*, John Wiley & Sons, New York, sixth edition, 1986.
[41] F. D. Murnaghan, Proc. Nat. Acad. Sci. USA **30** (1944) 244.
[42] C.-L. Fu and K.-M. Ho, Phys. Rev. B **28** (1983) 5480.
[43] D. Spišák, R. Lorenz, and J. Hafner, Phys. Rev. B **63** (2001) 094424.
[44] H. Over, H. Bludau, M. Skottke-Klein, G. Ertl, W. Moritz, and C. T. Campbell, Phys. Rev. B **45** (1992) 8638.
[45] P. Légaré, N. J. Castellani, and G. F. Cabeza, Surf. Sci. **496** (2002) L51.
[46] G. Chiarotti, editor, *Physics of Solid Surfaces. Subvolume b: Electronic and Vibrational Properties*, volume III.24 of *Landolt-Börnstein. Numerical Data and Functional Relationships in Science and Technology. New Series*, Springer, 1994.
[47] H. Steininger, S. Lehwald, and H. Ibach, Surf. Sci. **123** (1982) 1.
[48] A. C. Luntz, M. D. Williams, and D. S. Bethune, J. Chem. Phys. **89** (1988) 4381.
[49] W. Wurth, J. Stöhr, P. Feulner, X. Pan, K. R. Bauchspiess, Y. Baba, E. Hudel, G. Rocker, and D. Menzel, Phys. Rev. Lett. **65** (1990) 2426.
[50] U. Starke, N. Materer, A. Barbieri, R. Döll, K. Heinz,

M. A. Van Hove, and G. A. Somorjai, Surf. Sci. **287/288** (1993) 432.
[51] N. Materer, U. Starke, A. Barbieri, R. Döll, K. Heinz, M. A. Van Hove, and G. A. Somorjai, Surf. Sci. **325** (1995) 207.
[52] A. N. Artsyukhovich, V. A. Ukraintsev, and I. Harrison, Surf. Sci. **347** (1996) 303.
[53] U. Engström and R. Ryberg, Phys. Rev. Lett. **82** (1999) 2741.
[54] K. Gustafsson and S. Andersson, J. Chem. Phys. **120** (2004) 7750.
[55] P. J. Feibelman, S. Esch, and T. Michely, Phys. Rev. Lett. **77** (1996) 2257.
[56] P. J. Feibelman, Phys. Rev. B **56** (1997) 10532.
[57] P. J. Feibelman, J. Hafner, and G. Kresse, Phys. Rev. B **58** (1998) 2179.
[58] A. Eichler and J. Hafner, Phys. Rev. Lett. **79** (1997) 4481.
[59] A. Bogicevic, J. Strömquist, and B. I. Lundqvist, Phys. Rev. B **57** (1998) R4289.
[60] A. Kokalj, A. Lesar, M. Hodošček, and M. Causà, J. Phys. Chem. B **103** (1999) 7222.
[61] A. Eichler, F. Mittendorfer, and J. Hafner, Phys. Rev. B **62** (2000) 4744.
[62] A. Groß, A. Eichler, J. Hafner, M. J. Mehl, and D. A. Papaconstantopoulos, Surf. Sci. **539** (2003) L542.
[63] M. Lindroos, H. Pfnür, G. Held, and D. Menzel, Surf. Sci. **222** (1989) 451.
[64] C. Stampfl, S. Schwegmann, H. Over, M. Scheffler, and G. Ertl, Phys. Rev. Lett. **77** (1996) 3371.
[65] C. Stampfl and M. Scheffler, Phys. Rev. B **54** (1996) 2868.
[66] G. Herzberg and K. P. Huber, *Molecular Spectra and Molecular Structure. IV. Constants of Diatomic Molecules*, Van Nostrand Reinhold, 1979.
[67] B. Hammer, L. B. Hansen, and J. K. Nørskov, Phys. Rev. B **59** (1999) 7413.
[68] B. Hammer, Phys. Rev. Lett. **89** (2002) 016102.
[69] H. Ibach and D. L. Mills, *Electron energy loss spectroscopy and surface vibrations*, Academic Press, 1982.
[70] C. Puglia, A. Nilsson, B. Hernnäs, O. Karis, P. Bennich, and N. Mårtensson, Surf. Sci. **342** (1995) 119.
[71] P. D. Nolan, B. R. Lutz, P. L. Tanaka, J. E. Davis, and C. B. Mullins, Phys. Rev. Lett. **81** (1998) 3179.
[72] P. D. Nolan, B. R. Lutz, P. L. Tanaka, J. E. Davis, and C. B. Mullins, J. Chem. Phys. **111** (1999) 3696.
[73] P. Gambardella, Ž. Šljivančanin, B. Hammer, M. Blanc, K. Kuhnke, and K. Kern, Phys. Rev. Lett. **87** (2001) 056103.
[74] Ž. Šljivančanin and B. Hammer, Surf. Sci. **515** (2002) 235.
[75] A. Groß, *Theoretical surface science – A microscopic perspective*, Springer, Berlin, 2002.
[76] R. A. Sidik and A. B. Anderson, J. Electroanal. Chem. **528** (2002) 69.
[77] J. X. Wang and R. R. Markovic, N. M. Adžić, J. Phys. Chem. B **108** (2004) 4127.